Structure of the human Ccr4-Not nuclease module using X-ray crystallography and electron paramagnetic resonance spectroscopy distance measurements

Qionglin Zhang[1], Lorenzo Pavanello[2,%], Alexey Potapov[3,#], Mark Bartlam[1,#], and Gerlof Sebastiaan Winkler[2,#]

[1] Nankai International Advanced Research Institute (Shenzhen Futian); College of Life Sciences; State Key Laboratory of Medicinal Chemical Biology, Nankai University, Tianjin, 300071, China.

[2] School of Pharmacy, University of Nottingham, East Drive, University Park, Nottingham, NG7 2RD, U.K.

[3] School of Physics and Astronomy, Sir Peter Mansfield Imaging Centre, University of Nottingham, University Park, Nottingham, NG7 2RD, U.K.

[%] Present address: LifeArc, Stevenage Bioscience Catalyst Open Innovation Campus, Stevenage, SG1 2FX, UK

[#] To whom correspondence may be addressed: alexey.potapov@nottingham.ac.uk (AP), bartlam@nankai.edu.cn (MB), sebastiaan.winkler@nottingham.ac.uk (GSW).

Short title: Structure of the human Ccr4-Not nuclease module

Supplementary Material: Supplementary Material.pdf

Keywords:

RIDME; pulse EPR; mRNA; nuclease; Ccr4-Not; Caf1; CNOT7; Ccr4; CNOT6L; CNOT1

Abstract
Regulated degradation of mature, cytoplasmic mRNA is a key step in eukaryotic gene regulation. This process is typically initiated by the recruitment of deadenylase enzymes by cis-acting factors resulting in the shortening and removal of the 3’ poly(A) tail of the target mRNA. The Ccr4-Not complex, a major eukaryotic deadenylase, contains two exoribonuclease subunits with selectivity towards poly(A): Caf1 and Ccr4. The Caf1 deadenylase subunit binds the MIF4G domain of the large subunit CNOT1 (Not1) that is the scaffold of the complex. The Ccr4 nuclease is connected to the complex via its leucine-rich repeat (LRR) domain, which binds Caf1, whereas the catalytic activity of Ccr4 is provided by its EEP domain. While the relative positions of the MIF4G domain of CNOT1, the Caf1 subunit, and the LRR domain of Ccr4 are clearly defined in current models, the position of the EEP nuclease domain of Ccr4 is ambiguous. Here, we use X-ray crystallography, the AlphaFold resource of predicted protein structures, and pulse electron paramagnetic resonance spectroscopy to determine and validate the position of the EEP nuclease domain of Ccr4 resulting in an improved model of the human Ccr4-Not nuclease module.

Introduction

In eukaryotic cells, accurate control of gene expression requires the regulation of mRNA stability and translation in the cytoplasm. A key factor involved in these steps is the Ccr4-Not complex (1-5), which can be recruited to target mRNAs by cis-acting factors such as the A/U-rich binding protein TTP (6; 7), and the microRNA-repression complex (8; 9). In vertebrates, the Ccr4-Not complex can also interact with members of the BTG/TOB family of proteins (10; 11), including BTG2, which mediates interactions with cytoplasmic poly(A)-binding protein 1 and is frequently mutated in lymphoma (12-15).

The Ccr4-Not complex initiates mRNA degradation by shortening the mRNA poly(A) tail, which is often the rate-limiting step in the 5'-3' degradation pathway (1; 16; 3). Significant progress has been made towards understanding the structure of the Ccr4-Not complex, which is composed of eight subunits. The large subunit CNOT1 (Not1) forms the backbone of the complex that connects the remaining subunits. The catalytic activity, which selectively degrades poly(A), is confined to the nuclease sub-complex consisting of two subunits. The Caf1 subunit, which is encoded by the paralogues CNOT7 or CNOT8 in vertebrate cells, contains a catalytic DEDD domain and binds the MIF4G domain of CNOT1 (17-19). The Ccr4 nuclease, which in vertebrates is also encoded by two paralogues (CNOT6 and CNOT6L), contains a catalytic endonuclease-exonuclease-phosphatase (EEP) domain, and a leucine rich repeat (LRR) domain that interacts with the Caf1 subunit (20; 17; 21). Caf1 can also interact with the BTG domain of BTG/TOB proteins using an interface that does not overlap with residues interacting with the MIF4G domain of CNOT1 or the LRR domain of Ccr4 (22; 23).

Several studies showed that Caf1 and Ccr4 have distinct, but overlapping roles in cells (24-28). Biochemical studies using the purified complex, or the isolated nuclease sub-complex also showed a differential contribution of the subunits, although evidence for allosteric regulation has also been reported (29-33; 21). A model based on the X-ray structures of the yeast Not1(MIF4G)-Caf1-Ccr4 complex (17) and human CNOT6L (34) suggested interactions between the LRR of Ccr4 and the catalytic EEP domain and a distance of 60Å between the tightly-bound divalent metals in the catalytic sites of Caf1 and Ccr4 (17). By contrast, a recently reported structure of human Caf1/CNOT7-Ccr4/CNOT6 shows the distance to be notably shorter (46Å) (21). Moreover, no interactions between the EEP and LRR domains of Ccr4 were observed in the latter model, and the position of the EEP domain appeared to be determined by crystal packing contacts suggesting that the linker connecting the LRR and EEP domains is flexible (21).

Here, we report a structural model of the human nuclease module using a combination of X-ray crystallography and the AlphaFold predictive protein structure resource (35). In this structure, the position of the EEP domain of Ccr4 is notably different compared to the structures reported before. We then validated our structural model by distance measurements between divalent metal ions in the active sites of Caf1 and Ccr4 using pulse electron paramagnetic resonance (EPR) (36). The distance between the catalytic centres in our model correlated well with the experimental value indicating that the structure presented here represents an improved model of the human Ccr4-Not nuclease module.

Results and discussion

Crystal structure of the human CNOT1(MIF4G)-Caf1-Ccr4 nuclease module

To obtain a structure of the nuclease module of the human Ccr4-Not complex, we resolved a crystal structure of the CNOT1(MIF4G)-Caf1-Ccr4 ternary complex (**Figure 1A**) (**Table S1**). Clear electron density was visible for the MIF4G domain of CNOT1, Caf1 and the LRR domain of Ccr4 (**Figure 1A**). Unfortunately, the Ccr4 EEP nuclease domain could only be traced from residues 200-230, with the remainder of the domain not visible in electron density (**Figure S1**).

To provide information about the position of the Ccr4 EEP nuclease domain and to orient it relative to the LRR domain in the model, we superimposed the predicted AlphaFold model of human Ccr4 (35) onto the LRR domain Ccr4 in the ternary complex with an r.m.s.d. of 0.87 Å for 1,130 aligned atoms. The AlphaFold model shows high confidence in the relative positions of the LRR and nuclease domains (**Figure S2**) and aligns well with the EEP nuclease domain fragment from residues 200-230 (**Figure 1B**). Superimposing the AlphaFold model onto the LRR domain in the ternary complex enabled further assignment of residues 506-526 in the electron density.

The human CNOT1(MIF4G)-Caf1-Ccr4 complex structure was then used as a scaffold to assemble a model incorporating the metal ions in the Caf1 and Ccr4 active sites using the structures of CNOT1(MIF4G)-Caf1 (18) and of the EEP nuclease domain of Ccr4 (34). The CNOT1(MIF4G)-Caf1 binary structure (PDB ID: 4GMJ) was superimposed onto the ternary complex with an r.m.s.d. of 0.80 Å for 3,795 aligned atoms (**Figure 1C**). The structure of the EEP domain of Ccr4 (PDB ID: 3NGQ) was superimposed onto the AlphaFold model with an r.m.s.d. of 0.41 Å for 2,016 aligned atoms. In this model, the estimated distance between the tightly-bound Mg^{2+} ions in the active sites of Caf1 (coordinated by Asp40) and Ccr4 (coordinated by Glu240) is approximately 63.9 Å (**Figure 1C**).

A structure of the human Caf1-Ccr4 (CNOT6) dimeric complex was recently reported by Chen and colleagues (21). In this model, the Ccr4 EEP nuclease domain is in a notably different position with an estimated distance between the Mg^{2+} ions in Caf1 and Ccr4 of 46.4 Å (**Figure 1C**). This suggests that the EEP nuclease domain of Ccr4 may be flexible in solution although it should be noted that when the Ccr4-Caf1 binary structure (PDB ID: 7AX1) is superimposed onto the CNOT1(MIF4G)-Caf1-Ccr4 complex, the Ccr4 nuclease domain in the binary complex clashes with CNOT1(MIF4G) in the ternary complex (**Figure S3**). Thus, the orientation of the EEP domain of Ccr4 with respect to Caf1 and the LLR domain of Ccr4 in the dimeric complex reported by Chen et al. (21) is unlikely to represent the conformation of the EEP nuclease domain in the context of larger Ccr4-Not complexes. Thus, the position of the EEP domain of Ccr4 may be restricted by other subunits of the Ccr4-Not complex. Alternatively, the position of the EEP nuclease domain of Ccr4 with respect to the LLR domain of Ccr4 may be more defined as predicted by the AlphaFold model (**Figure S2**).

A structure of the yeast Not1(MIF4G)-Caf1-Ccr4 complex has also been reported, albeit with a partially resolved Ccr4 EEP nuclease domain, reflecting the poor ordering of Ccr4-Not nuclease complex crystals (17). In the absence of a complete structure of the Ccr4 nuclease domain, superimposing the human Ccr4 nuclease domain onto the partial yeast structure (PDB ID: 4B8C; r.m.s.d. of 0.95 Å for 415 aligned atoms) yields an estimated distance

between Mg^{2+} ions in Ccr4 and Caf1 of 59.7 Å (**Figure 1D**). However, the orientation of the EEP nuclease domain of Ccr4 is rotated by 28° compared to the structure presented here.

Distance measurements between divalent metal ions in the active sites of Caf1 and Ccr4
To provide further experimental evidence for the model of the nuclease sub-complex presented here, we carried out pulse electron paramagnetic resonance (EPR) experiments to measure the distance between the metal-binding sites of Caf1 and Ccr4. To determine whether the EEP domain of Ccr4 is flexible, or restricted by the LLR domain of Ccr4, we used a trimeric BTG2-Caf1-Ccr4 complex for these experiments (29). This complex lacks the MIF4G domain of CNOT1 and would allow the orientation of the EEP domain of Ccr4 as reported in the structure of the human dimeric Caf1-Ccr4 complex (**Figure S3**) (21). After purification of the apo-complex lacking metal ions, the protein complex was incubated in the presence of paramagnetic Mn^{2+} ions to make the sample suitable for EPR studies. Under the conditions used, the nuclease sites in Caf1 and Ccr4 are expected to be populated by only a single Mn^{2+} ion each (**Supplementary Results, Figure S4**) (37; 34).

To measure the distance between the Mn^{2+} ions in the active sites of Caf1 and Ccr4, a RIDME (relaxation-induced dipolar modulation) experiment (36) was carried using a three pulse sequence $\frac{\pi}{2} - t - \frac{\pi}{2} - \tau - \pi - t -$ echo (**Figure S5**). The spin echo intensity $S(t)$ is recorded as a function of evolution time t – a delay between the first and the second pulse, while the mixing time τ between the second and third pulses is kept constant. The spin echo intensity $S(t)$ undergoes dephasing due to spontaneous flips of the dipolar coupled neighbouring electron spins during the mixing interval, therefore for brevity $S(t)$ is further referred to as the dephasing curve. To exclude signal loss due to other sources unrelated to the electron spin dipolar interaction (e.g. dephasing due to flips of neighbouring nuclei), the dephasing curves $S(t)$ recorded with long mixing times of $\tau = 50$ µs and $\tau = 180$ µs were normalized by a dephasing curve $S_0(t)$ recorded with a short mixing time of $\tau = 10$ µs. The background corrected normalized dephasing curves are shown in **Figure 1E**.

The RIDME dephasing curves of Mn^{2+} pairs in BTG2-Caf1-Ccr4 arise due to neighbouring spin flips with $\Delta M_S = \pm 1$, and due to flips with $\Delta M_S = \pm 2, \pm 3, \pm 4, \pm 5$, also known as overtones (38-40). A somewhat faster decay of RIDME dephasing curve is observed with $\tau = 180$ µs compared to the one with $\tau = 50$ µs (**Figure 1E**), suggesting a larger contribution of higher overtones in the former. A significant contribution of $\Delta M_S = \pm 2$ was previously found even with short mixing times (38). Therefore, the overtone weights should be specific to a particular ligand structure of a paramagnetic site, and these weights can be found using calibration with model compounds (40; 41). However, distance distributions can be evaluated even without such information. A *lower bound* on the distance between a pair of Mn^{2+} in BTG2-Caf1-Ccr4 can be obtained by modelling the $\tau = 50$ µs RIDME dephasing curve by a Gaussian distance distribution without any overtones. Such model produces a Mn^{2+}-Mn^{2+} distance distribution centred at 64.2±0.3 Å with a full width at half height of 18.2±1.2 Å (**Figure S6**).

A better estimate of the distance between a pair of Mn^{2+} in BTG2-Caf1-Ccr4 can be obtained by finding a Gaussian distance distribution that fits both RIDME dephasing curves (with $\tau = 50$ µs and with $\tau = 180$ µs) concurrently. Only the contributions with $\Delta M_S = \pm 1$ (i.e. the base contribution with a dipolar frequency) and $\Delta M_S = \pm 2$ (i.e. the first overtone with double dipolar frequency) are taken into account, because previous work demonstrated them to be

dominant (39; 40). The inset in **Figure 1E** shows the resulting distance distribution with shaded areas showing the 68% confidence intervals. Such model gives an estimated distribution between the Mn^{2+} ions in two nucleases centred at 64.9 ± 1.7 Å, with the full width at half height of 14.4 ± 2.1 Å. The weights of the overtones are summarized in **Table S3**.

Conclusion

The distance between the catalytic centres in the X-ray model of the CNOT1(MIF4G)-Caf1-Ccr4 nuclease module presented here (63.9Å) is in good agreement with the experimental distance measurement (64.9 ± 1.7Å). This indicates that the structure presented here provides an improved model of the human Ccr4-Not nuclease module that is notably different regarding the position of the EEP nuclease domain of Ccr4 compared to previous models (17; 21).

Materials and methods

Protein expression and purification

For protein crystallization, full length human Caf1/CNOT7 and Ccr4/CNOT6L were co-expressed using the Bac-to-Bac Baculovirus Expression System in Sf9 insect cells. The human CNOT1 MIF4G domain (residues 1093-1317) was expressed in *E. coli* BL21 (DE3). For electron paramagnetic resonance spectroscopy, the BTG2-Caf1-Ccr4 trimeric human nuclease complex was purified as described (42) with modifications (**Supplementary Data**).

Crystallization and data collection

The CNOT1(MIF4G)-Caf1-Ccr4 complex was concentrated to 2.5 mg ml^{-1} and 5 mg ml^{-1} for crystallization. Crystals were grown at 293K using the sitting-drop vapour-diffusion method from a condition containing 0.1 M MES pH 6.5, 12% PEG20000. After optimization, the best crystals were grown in 0.1 M MES pH 6.0, 8% PEG20000. Crystals were cryoprotected by soaking in crystallization solution containing 30% glycerol, then flash-cooled in liquid nitrogen prior to data collection. Diffraction data were collected at 100 K on beamline BL18U1 of the Shanghai Synchrotron Radiation Facility (SSRF). All diffraction data were processed by the HKL2000 suite (43).

Structure determination

The human CNOT1(MIF4G)-Caf1-Ccr4 complex structure was solved by molecular replacement using the PHASER (44) program in PHENIX (45) with structures of the yeast Ccr4 LRR domain (PDB ID: 4B8C), CNOT1 MIF4G domain (PDB ID: 4GMJ) and Caf1 (PDB ID: 4GMJ) used as ensemble search models. Refinement of the structures was carried out using PHENIX (45) and manual rebuilding was performed in Coot (46). Structures were validated by MolProbity (47). The AlphaFold model of human CNOT6L (Uniprot Q96LI5) was downloaded from the EMBL-EBI repository (https://www.alphafold.ebi.ac.uk/) (35). All structure figures were drawn using PyMOL (48).

Pulse EPR measurements

All EPR measurements were carried out at a temperature of ~30 K using a W-band pulse EPR spectrometer described before (49). The RIDME pulse sequence $\frac{\pi}{2} - t - \frac{\pi}{2} - \tau - \pi - t -$ echo employed microwave pulses with durations $t_{\frac{\pi}{2}} / t_{\pi} = 20/40$ µs. The magnetic field for collecting RIDME data was set at the first line of Mn^{2+} sextet as labelled in **Figure S4**. RIDME datasets consisted of 80 time points with the maximum evolution time t of ~4 ms. To

save experimental time, the RIDME dephasing curves were recorded with variable number of scans at each point, such that points corresponding to larger evolution times t have more scans. The total experimental time for recording each dephasing curve was typically 3-5 hours.

Data processing was carried out using custom Python scripts. Data fitting used the Powell minimization algorithm implemented in the *scipy* library. Confidence bounds for the distance distribution and other parameters were obtained by analysing an ensemble of DEER traces generated using resampling with replacement (50).

Data availability

Atomic coordinates and structure factors for the reported crystal structure have been deposited with the Protein Data Bank (51) under accession number 7VOI.

Supplementary material

Supplementary material is available online and contains supplementary materials and methods, and supplementary results.

Acknowledgements

This work was supported by a Vice-Chancellor's scholarship for research excellence (L.P.) and the Faculty of Science Enhancement Fund (A.P. and G.S.W.); by the National Key Research and Development Program of China (grant number 2020YFC1807003 to M.B.); and by the National Natural Science Foundation of China (grant numbers 31870053 to M.B. and 31800627 to Q.Z.).

Conflict of interest

The Authors declare that there is no conflict of interest.

Figure

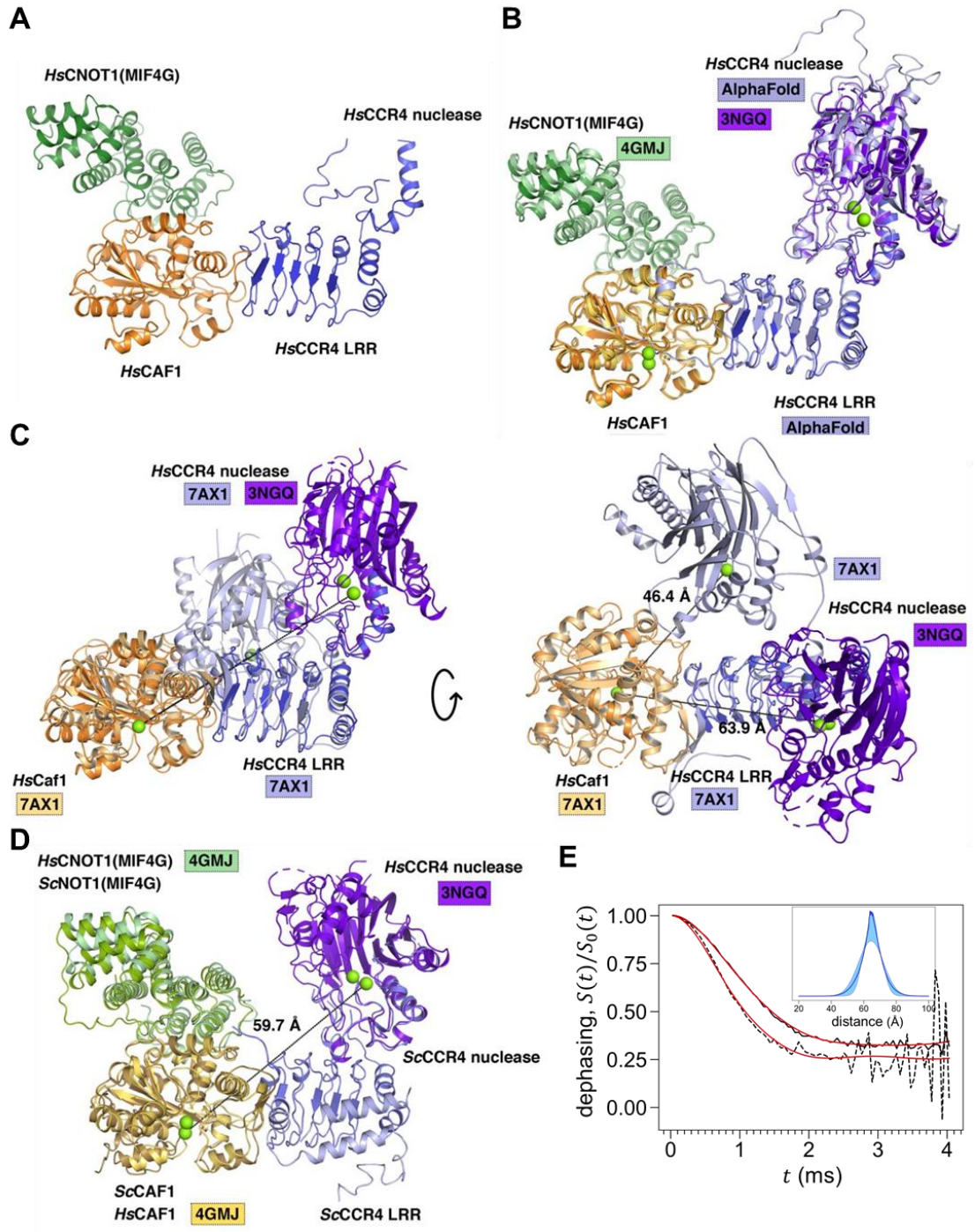

Figure 1. Structure of the human Ccr4-Not nuclease module. (A) Crystal structure of the human (*Hs*) Ccr4-Not nuclease domain containing the MIF4G domain of CNOT1 (*green*), Caf1 (*orange*) and Ccr4 (*blue*). **(B)** Superimposition of the structure of the human (*Hs*) CNOT1(MIF4G)-Caf1 complex (PDB ID: 4GMJ) (18), the AlphaFold model of human Ccr4 (35), and the structure of the nuclease domain of human Ccr4 (PDB ID: 3NGQ) (34) on the crystal structure of the nuclease module. Divalent metal ions in the active sites of Caf1 and Ccr4 are shown (*bright green*). **(C)** Superimposition of the structure of the human (*Hs*) Caf1-Ccr4 complex (PDB ID: 7AX1) (21) with the structure of the nuclease complex, viewed from the side (*left panel*) and the top (*right panel*). The MIF4G domain of CNOT1 is omitted for

clarity. Active-site divalent metal ions (*bright green*) in Caf1 and Ccr4 are indicated. The distances between the metal ions in the high affinity binding sites of Caf1 and Ccr4 are shown (37; 34). **(D)** Superimposition of the structure of the human (*Hs*) CNOT1(MIF4G)-Caf1 complex (PDB ID: 4GMJ) (18), and the structure of the nuclease domain of human Ccr4 (PDB ID: 3NGQ) (34) on the crystal structure of the yeast *Saccharomyces cerevisiae* (*Sc*) Not1(MIF4G)-Caf1-Ccr4 nuclease module (PDB ID: 4B8C) (17). Active-site divalent metal ions (*bright green*) in Caf1 and Ccr4 are indicated. The distance between the metal ions in the high affinity binding sites of Caf1 and Ccr4 is shown (37; 34). **(E)** Normalized and background corrected RIDME trace for Mn^{2+} bound to the BTG2-Caf1-Ccr4 complex, the mixing time τ=50 µs (*solid black line*) and τ=180µs (*dashed black line*). The best fit results (*red*) were obtained using the distance distribution shown in the inset. The distance distribution (*inset, solid blue*) and the confidence interval corresponding to 68% (*inset, light blue shade*) are also shown.

References

1. Parker R, Song H (2004) The enzymes and control of eukaryotic mRNA turnover. Nature Struct Mol Biol 11:121-127.
2. Collart MA, Panasenko OO (2012) The Ccr4-not complex. Gene 492:42-53. PMID: 22027279
3. Wahle E, Winkler GS (2013) RNA decay machines: Deadenylation by the Ccr4-Not and Pan2-Pan3 complexes. Biochim Biophys Acta 1829:561-570. PMID: 23337855
4. Temme C, Simonelig M, Wahle E (2014) Deadenylation of mRNA by the CCR4-NOT complex in Drosophila: molecular and developmental aspects. Front Genet 5:143. PMID: 24904643
5. Xu K, Bai Y, Zhang A, Zhang Q, Bartlam MG (2014) Insights into the structure and architecture of the CCR4-NOT complex. Front Genet 5:137. PMID: 24904637
6. Sandler H, Kreth J, Timmers HT, Stoecklin G (2011) Not1 mediates recruitment of the deadenylase Caf1 to mRNAs targeted for degradation by tristetraprolin. Nucleic Acids Res 39:4373-4386. PMID: 21278420
7. Fabian MR, Frank F, Rouya C, Siddiqui N, Lai WS, Karetnikov A, Blackshear PJ, Nagar B, Sonenberg N (2013) Structural basis for the recruitment of the human CCR4-NOT deadenylase complex by tristetraprolin. Nature structural & molecular biology 20:735-739. PMID: 23644599
8. Behm-Ansmant I, Rehwinkel J, Doerks T, Stark A, Bork P, Izaurralde E (2006) mRNA degradation by miRNAs and GW182 requires both CCR4:NOT deadenylase and DCP1:DCP2 decapping complexes. Genes & development 20:1885-1898. PMID: 16815998
9. Piao X, Zhang X, Wu L, Belasco JG (2010) CCR4-NOT deadenylates mRNA associated with RNA-induced silencing complexes in human cells. Molecular and cellular biology 30:1486-1494. PMID: 20065043
10. Mauxion F, Chen CY, Seraphin B, Shyu AB (2009) BTG/TOB factors impact deadenylases. Trends Biochem Sci 34:640-647. PMID: 19828319
11. Winkler GS (2010) The mammalian anti-proliferative BTG/Tob protein family. J Cell Physiol 222:66-72.
12. Morin RD, Mendez-Lago M, Mungall AJ, Goya R, Mungall KL, Corbett RD, Johnson NA, Severson TM, Chiu R, Field M, Jackman S, Krzywinski M, Scott DW, Trinh DL, Tamura-Wells J, Li S, Firme MR, Rogic S, Griffith M, Chan S, Yakovenko O, Meyer IM, Zhao EY, Smailus D, Moksa M, Chittaranjan S, Rimsza L, Brooks-Wilson A, Spinelli JJ, Ben-Neriah S, Meissner B, Woolcock B, Boyle M, McDonald H, Tam A, Zhao Y, Delaney A, Zeng T, Tse K, Butterfield Y, Birol I, Holt R, Schein J, Horsman DE, Moore R, Jones SJ, Connors JM, Hirst M, Gascoyne RD, Marra MA (2011) Frequent mutation of histone-modifying genes in non-Hodgkin lymphoma. Nature 476:298-303. PMID: 21796119
13. Stupfler B, Birck C, Seraphin B, Mauxion F (2016) BTG2 bridges PABPC1 RNA-binding domains and CAF1 deadenylase to control cell proliferation. Nat Commun 7:10811. PMID: 26912148
14. Reddy A, Zhang J, Davis NS, Moffitt AB, Love CL, Waldrop A, Leppa S, Pasanen A, Meriranta L, Karjalainen-Lindsberg ML, Nørgaard P, Pedersen M, Gang AO, Høgdall E, Heavican TB, Lone W, Iqbal J, Qin Q, Li G, Kim SY, Healy J, Richards KL, Fedoriw Y, Bernal-Mizrachi L, Koff JL, Staton AD, Flowers CR, Paltiel O, Goldschmidt N, Calaminici M, Clear A, Gribben J, Nguyen E, Czader MB, Ondrejka SL, Collie A, Hsi ED, Tse E, Au-Yeung RKH, Kwong YL, Srivastava G, Choi WWL, Evens AM, Pilichowska M, Sengar M, Reddy N, Li S, Chadburn A, Gordon LI, Jaffe ES, Levy S, Rempel R, Tzeng T, Happ LE, Dave T, Rajagopalan D, Datta J, Dunson DB, Dave SS

(2017) Genetic and Functional Drivers of Diffuse Large B Cell Lymphoma. Cell 171:481-494.e415. PMID: 28985567
15. Almasmoum HA, Airhihen B, Seedhouse C, Winkler GS (2021) Frequent loss of BTG1 activity and impaired interactions with the Caf1 subunit of the Ccr4-Not deadenylase in non-Hodgkin lymphoma. Leuk Lymphoma 62:281-290. PMID: 33021411
16. Goldstrohm AC, Wickens M (2008) Multifunctional deadenylase complexes diversify mRNA control. Nat Rev Mol Cell Biol 9:337-344. PMID: 18334997
17. Basquin J, Roudko VV, Rode M, Basquin C, Seraphin B, Conti E (2012) Architecture of the nuclease module of the yeast Ccr4-not complex: the Not1-Caf1-Ccr4 interaction. Mol Cell 48:207-218. PMID: 22959269
18. Petit AP, Wohlbold L, Bawankar P, Huntzinger E, Schmidt S, Izaurralde E, Weichenrieder O (2012) The structural basis for the interaction between the CAF1 nuclease and the NOT1 scaffold of the human CCR4-NOT deadenylase complex. Nucleic Acids Res 40:11058-11072. PMID: 22977175
19. Bawankar P, Loh B, Wohlbold L, Schmidt S, Izaurralde E (2013) NOT10 and C2orf29/NOT11 form a conserved module of the CCR4-NOT complex that docks onto the NOT1 N-terminal domain. RNA biology 10:228-244. PMID: 23303381
20. Dupressoir A, Morel AP, Barbot W, Loireau MP, Corbo L, Heidmann T (2001) Identification of four families of yCCR4- and Mg^{2+}-dependent endonuclease-related proteins in higher eukaryotes, and characterization of orthologs of yCCR4 with a conserved leucine-rich repeat essential for hCAF1/hPOP2 binding. BMC Genomics 2:9. PMID: 11747467
21. Chen Y, Khazina E, Izaurralde E, Weichenrieder O (2021) Crystal structure and functional properties of the human CCR4-CAF1 deadenylase complex. Nucleic Acids Res 49:6489-6510. PMID: 34038562
22. Yang X, Morita M, Wang H, Suzuki T, Yang W, Luo Y, Zhao C, Yu Y, Bartlam M, Yamamoto T, Rao Z (2008) Crystal structures of human BTG2 and mouse TIS21 involved in suppression of CAF1 deadenylase activity. Nucleic Acids Res 36:6872-6881. PMID: 18974182
23. Horiuchi M, Takeuchi K, Noda N, Muroya N, Suzuki T, Nakamura T, Kawamura-Tsuzuku J, Takahasi K, Yamamoto T, Inagaki F (2009) Structural basis for the antiproliferative activity of the Tob-hCaf1 complex. J Biol Chem 284:13244-13255. PMID: 19276069
24. Aslam A, Mittal S, Koch F, Andrau JC, Winkler GS (2009) The Ccr4-Not Deadenylase Subunits CNOT7 and CNOT8 Have Overlapping Roles and Modulate Cell Proliferation. Mol Biol Cell 20:3840-3850.
25. Mittal S, Aslam A, Doidge R, Medica R, Winkler GS (2011) The Ccr4a (CNOT6) and Ccr4b (CNOT6L) deadenylase subunits of the human Ccr4-Not complex contribute to the prevention of cell death and senescence. Mol Biol Cell 22:748-758.
26. Webster MW, Chen YH, Stowell JAW, Alhusaini N, Sweet T, Graveley BR, Coller J, Passmore LA (2018) mRNA Deadenylation Is Coupled to Translation Rates by the Differential Activities of Ccr4-Not Nucleases. Mol Cell 70:1089-1100 e1088. PMID: 29932902
27. Yi H, Park J, Ha M, Lim J, Chang H, Kim VN (2018) PABP Cooperates with the CCR4-NOT Complex to Promote mRNA Deadenylation and Block Precocious Decay. Mol Cell 70:1081-1088 e1085. PMID: 29932901
28. Mostafa D, Takahashi A, Yanagiya A, Yamaguchi T, Abe T, Kureha T, Kuba K, Kanegae Y, Furuta Y, Yamamoto T, Suzuki T (2020) Essential functions of the CNOT7/8 catalytic subunits of the CCR4-NOT complex in mRNA regulation and cell viability. RNA Biol 17:403-416. PMID: 31924127

29. Maryati M, Airhihen B, Winkler GS (2015) The enzyme activities of Caf1 and Ccr4 are both required for deadenylation by the human Ccr4-Not nuclease module. Biochem J 469:169-176. PMID: 25944446
30. Niinuma S, Fukaya T, Tomari Y (2016) CCR4 and CAF1 deadenylases have an intrinsic activity to remove the post-poly(A) sequence. RNA 22:1550-1559. PMID: 27484313
31. Stowell JAW, Webster MW, Kogel A, Wolf J, Shelley KL, Passmore LA (2016) Reconstitution of Targeted Deadenylation by the Ccr4-Not Complex and the YTH Domain Protein Mmi1. Cell Rep 17:1978-1989. PMID: 27851962
32. Airhihen B, Pavanello L, Jadhav GP, Fischer PM, Winkler GS (2019) 1-Hydroxy-xanthine derivatives inhibit the human Caf1 nuclease and Caf1-containing nuclease complexes via Mg^{2+}-dependent binding. FEBS Open Bio 9:717-727. PMID: 30984545
33. Raisch T, Chang CT, Levdansky Y, Muthukumar S, Raunser S, Valkov E (2019) Reconstitution of recombinant human CCR4-NOT reveals molecular insights into regulated deadenylation. Nat Commun 10:3173. PMID: 31320642
34. Wang H, Morita M, Yang X, Suzuki T, Yang W, Wang J, Ito K, Wang Q, Zhao C, Bartlam M, Yamamoto T, Rao Z (2010) Crystal structure of the human CNOT6L nuclease domain reveals strict poly(A) substrate specificity. EMBO J 29:2566-2576.
35. Jumper J, Evans R, Pritzel A, Green T, Figurnov M, Ronneberger O, Tunyasuvunakool K, Bates R, Žídek A, Potapenko A, Bridgland A, Meyer C, Kohl SAA, Ballard AJ, Cowie A, Romera-Paredes B, Nikolov S, Jain R, Adler J, Back T, Petersen S, Reiman D, Clancy E, Zielinski M, Steinegger M, Pacholska M, Berghammer T, Bodenstein S, Silver D, Vinyals O, Senior AW, Kavukcuoglu K, Kohli P, Hassabis D (2021) Highly accurate protein structure prediction with AlphaFold. Nature 596:583-589.
36. Kulik LV, Dzuba SA, Grigoryev IA, Tsvetkov YD (2001) Electron dipole–dipole interaction in ESEEM of nitroxide biradicals. Chem Phys Lett 343:315-324.
37. Andersen KR, Jonstrup AT, Van LB, Brodersen DE (2009) The activity and selectivity of fission yeast Pop2p are affected by a high affinity for Zn^{2+} and Mn^{2+} in the active site. RNA 15:850-861.
38. Razzaghi S, Qi M, Nalepa AI, Godt A, Jeschke G, Savitsky A, Yulikov M (2014) RIDME Spectroscopy with Gd(III) Centers. J Phys Chem Lett 5:3970-3975. PMID: 26276479
39. Akhmetzyanov D, Ching HY, Denysenkov V, Demay-Drouhard P, Bertrand HC, Tabares LC, Policar C, Prisner TF, Un S (2016) RIDME spectroscopy on high-spin Mn^{2+} centers. Phys Chem Chem Phys 18:30857-30866. PMID: 27801444
40. Keller K, Zalibera M, Qi M, Koch V, Wegner J, Hintz H, Godt A, Jeschke G, Savitsky A, Yulikov M (2016) EPR characterization of Mn(ii) complexes for distance determination with pulsed dipolar spectroscopy. Phys Chem Chem Phys 18:25120-25135. PMID: 27711532
41. Keller K, Mertens V, Qi M, Nalepa AI, Godt A, Savitsky A, Jeschke G, Yulikov M (2017) Computing distance distributions from dipolar evolution data with overtones: RIDME spectroscopy with Gd(iii)-based spin labels. Phys Chem Chem Phys 19:17856-17876. PMID: 28660955
42. Pavanello L, Hall B, Airhihen B, Winkler GS (2018) The central region of CNOT1 and CNOT9 stimulate deadenylation by the Ccr4-Not nuclease module. Biochem J 475:3437-3450.
43. Otwinowski Z, Minor W (1997) Processing of X-ray diffraction data collected in oscillation mode. Methods Enzymol 276:307-326. PMID: 27754618
44. McCoy AJ, Grosse-Kunstleve RW, Adams PD, Winn MD, Storoni LC, Read RJ (2007) Phaser crystallographic software. J Appl Crystallogr 40:658-674. PMID: 19461840
45. Adams PD, Afonine PV, Bunkóczi G, Chen VB, Davis IW, Echols N, Headd JJ, Hung LW, Kapral GJ, Grosse-Kunstleve RW, McCoy AJ, Moriarty NW, Oeffner R, Read RJ,

Richardson DC, Richardson JS, Terwilliger TC, Zwart PH (2010) PHENIX: a comprehensive Python-based system for macromolecular structure solution. Acta Crystallogr D Biol Crystallogr 66:213-221. PMID: 20124702
46. Emsley P, Lohkamp B, Scott WG, Cowtan K (2010) Features and development of Coot. Acta Crystallogr D Biol Crystallogr 66:486-501. PMID: 20383002
47. Chen VB, Arendall WB, 3rd, Headd JJ, Keedy DA, Immormino RM, Kapral GJ, Murray LW, Richardson JS, Richardson DC (2010) MolProbity: all-atom structure validation for macromolecular crystallography. Acta Crystallogr D Biol Crystallogr 66:12-21. PMID: 20057044
48. Schrödinger LLC The PyMOL Molecular Graphics System, Version 2.4.2.
49. Gennaro A, Karabanov A, Potapov A, Kockenberger W (2020) Heteronuclear DNP of ^{1}H and ^{19}F nuclei using BDPA as a polarizing agent. Phys Chem Chem Phys 22:7803-7816. PMID: 32249877
50. Potapov A (2020) Application of spherical harmonics for DEER data analysis in systems with a conformational distribution. J Magn Reson 316:106769. PMID: 32574865
51. Berman H, Henrick K, Nakamura H (2003) Announcing the worldwide Protein Data Bank. Nat Struct Biol 10:980. PMID: 14634627

Supplementary Material

Structure of the human Ccr4-Not nuclease module using x-ray crystallography and electron paramagnetic resonance spectroscopy distance measurements

Qionglin Zhang[1], Lorenzo Pavanello[2,%], Alexey Potapov[3,#], Mark Bartlam[1,#], and Gerlof Sebastiaan Winkler[2,#]

[1] Nankai International Advanced Research Institute (Shenzhen Futian); College of Life Sciences; State Key Laboratory of Medicinal Chemical Biology, Nankai University, Tianjin, 300071, China.

[2] School of Pharmacy, University of Nottingham, East Drive, University Park, Nottingham, NG7 2RD, U.K.

[3] School of Physics and Astronomy, Sir Peter Mansfield Imaging Centre, University of Nottingham, University Park, Nottingham, NG7 2RD, U.K.

Table of Contents

Supplementary results

EPR spectroscopy

The field-sweep EPR spectra of high-spin (electron spin S=5/2) Mn^{2+} ion in an aqueous solution and in a complex with BTG2-Caf1-Ccr4 protein reveal multiplets of six sharp lines superimposed onto a broad background (shown in **Fig. S4**). The sharp lines arise due to the electron spin transitions with $|M_S = -\frac{1}{2}, M_I\rangle \leftrightarrow |M_S = \frac{1}{2}, M_I\rangle$, where M_S and M_I are the projections of the electron and Mn^{2+} nuclear spins (I=5/2) respectively. The splitting between the six lines is given by the hyperfine (HF) interaction with Mn^{2+} nuclear spin. The width of each sharp line depends on the zero-field splitting (ZFS) interaction in the second order of perturbation theory (1). The broad background, on which the sextet of lines is superimposed, arises from electron spin transitions $|M_S, M_I\rangle \leftrightarrow |M_S + 1, M_I\rangle$ with $M_S \neq \frac{1}{2}$.

Both the Mn^{2+} HF and ZFS interactions are magnetic parameters, the magnitudes of which depend on the positions and type of ligands around Mn^{2+} ion. The splitting between the six lines and the their width change when Mn^{2+} ions in an aqueous solution are added to a solution containing BTG2-Caf1-Ccr4 (final concentrations $[Mn^{2+}] \approx [BTG2\text{-}Caf1\text{-}Ccr4] \approx 0.1$ mM). Such a difference in the HF and ZFS interactions implies that Mn^{2+} ions bind well to the protein complex (parameters extracted from the spectra in **Fig. S4** are summarized in **Table S2**). Upon such binding, no free Mn^{2+} remains in the solution, because the field-sweep spectra feature only one set of hyperfine splittings. In addition, the field-sweep spectra show no features corresponding to a nuclease site with a pair of occupying Mn^{2+} ions (2). This finding agrees with the notion that one metal ion in Caf1 and Ccr4 is bound with high affinity, and the second with low affinity (3; 4). Such result is also supported by a previous EPR study of Mn^{2+} binding to a nuclease site in DNA-polymerase (5). There it was shown that the two ion binding sites in the nuclease have significantly different binding constants of about ~10 μM and ~1000 μM for the "tight" and "weak" sites respectively. Therefore, given the concentrations of both the [BTG2-Caf1-Ccr4] and $[Mn^{2+}] \approx 100$ μM, the nuclease sites in BTG2-Caf1-Ccr4 are expected to be populated only by a single Mn^{2+} ion each.

Supplementary materials and methods

Protein expression and purification

For protein crystallization, full length human Caf1/CNOT7 and Ccr4/CNOT6L were co-expressed using the Bac-to-Bac Baculovirus Expression System in Sf9 insect cells. Both cDNAs were cloned with a glutathione S-transferase tag into the pFastBac vector (Invitrogen) to obtain the Bacmid. A cDNA encoding the human CNOT1 MIF4G domain (residues 1093-1317) was cloned into the pGEX-6p-1 vector (GE Healthcare) and expressed in *E. coli* BL21 (DE3). Caf1-Ccr4 and CNOT1(MIF4G) were first purified by glutathione affinity chromatography. PreScission Protease was then used to remove the glutathione S-transferase tags. Caf1-Ccr4 and CNOT1(MIF4G) were then mixed in a 1:1 molar ratio overnight at 4°C and further purified on a HiLoad 16/60 Superdex 200 column (GE Healthcare) to obtain the CNOT1(MIF4G)-Caf1-Ccr4 ternary complex.

For electron paramagnetic resonance spectroscopy, the BTG2–Caf1–Ccr4 trimeric human nuclease complex was purified as described (6) with modifications. Briefly, the trimeric complex was expressed in *E. coli* BL21 (DE3) transformed with plasmids pACYC-Duet-1-

StrepII-CNOT6L-CNOT7 and pQE80L-BTG2. Soluble lysates were loaded onto a 1 ml Strep-Tactin sepharose gravity column (IBA LifeSciences) and eluted with buffer SB (20 mM Tris–HCl pH 7.8, 250 mM NaCl, 10% glycerol, 1 mM β-mercaptoethanol, 10 mM D-Desthiobiotin) to isolate trimeric StrepII·Ccr4–Caf1–His·BTG2 complexes. Peak fractions were further purified by size-exclusion chromatography (HiPrep 16/60 Sephacryl S-200 HR column, GE Healthcare) equilibrated and eluted in buffer GF (50 mM Tris–HCl pH 7.9, 250 mM NaCl, 5% glycerol, 1 mM β-mercaptoethanol). Peak fractions were pooled, and buffer was exchanged using a PD-10 column (GE Healthcare) to 50 mM Tris–HCl pH 7.9, 250 mM NaCl, 1 mM β-mercaptoethanol prepared using D_2O. Proteins were concentrated using a Vivaspin concentrator (Sartorius) to a final concentration of 17.6 mg/ml (25 μL). After addition of an equimolar $MnCl_2$ concentration (150 mM, 1 μL), 8.4 mg deuterated glycerol (glycerol-D8) was added to a final concentration of 19% (v/v). Purified proteins (5 μL) were transferred to sample tubes and stored in liquid nitrogen.

Supplementary tables

Table S1. Data collection and refinement statistics.

Data collection	
Space group	$P4_12_12$
a, b, c (Å)	111.0, 111.0, 242.9
α, β, γ (°)	90, 90, 90
Resolution (Å)[b]	50.00-4.40 (4.48-4.40)
Total reflections	126,351
Unique reflections[b]	10,302 (493)
Average I/σ (I)[b]	27.3 (4.7)
[a]R_{pim} (%)	5.0 (17.7)
$CC_{1/2}$(%)	99.9 (92.6)
Redundancy[b]	12.3 (11.3)
Completeness (%)[b]	100.0 (100.0)
Wilson B factor (Å^2)	162.0
Refinement	
Resolution (Å)	38.74-4.40 (4.54-4.40)
Completeness (%)	97.5 (90.2)
No. of reflections used in refinement	10,103 (896)
R_{work} / R_{free} (%)	26.3 / 32.4
No. of non-H atoms	
Protein	5,449
R.m.s. deviations	
bond length (Å)	0.006
bond angle (°)	0.97
Average B value (Å^2)	
Protein	198.0
Ramachandran plot	
Favoured (%)	92.0
Allowed (%)	5.8
Outliers (%)	2.3

[a] $R_{pim} = \Sigma_h[1/(n_h-1)]^{1/2} \Sigma_i |\langle I_h\rangle - I_{h,i}| / \Sigma_h\Sigma_i I_{h,i}$. [b] Data in parentheses correspond to the highest-resolution shell.

Table S2. Summary of spectral parameters of Mn^{2+} ions in an aqueous solution of $MnCl_2$ and Mn^{2+} bound to BTG2-Caf1-Ccr4.

	Mn^{2+} hyperfine coupling (MHz)	**Mn^{2+} sextet line FWHH[a] (MHz)**
Mn^{2+} (aq.)	269.5±0.6	36±1
Mn^{2+} - BTG2-Caf1-Ccr4	264.0±0.8	41±1

[a] Full-width at half height

Table S3. Summary of parameters. Parameters were obtained using the procedure (described in the main text) for simultaneous fitting of the datasets shown in Fig. 1. Only the weights of the first overtone P_2 ($\Delta M_S = \pm 2$) are reported because the weight of the base contribution P_1 ($\Delta M_S = \pm 1$) satisfies $P_1 + P_2 = 1$.

Gaussian distribution centre	6.49±0.17 nm
Gaussian distribution FWHH[a]	1.44±0.21 nm
weight of the first overtone ($\Delta M_S = \pm 2$)for the RIDME[b] trace with $\tau = 50$ µs	0.11±0.07
weight of the first overtone ($\Delta M_S = \pm 2$) for the RIDME[b] trace with $\tau = 180$ µs	0.32±0.13

[a] Full-width at half height
[b] Relaxation-induced dipolar modulation

Supplementary figures

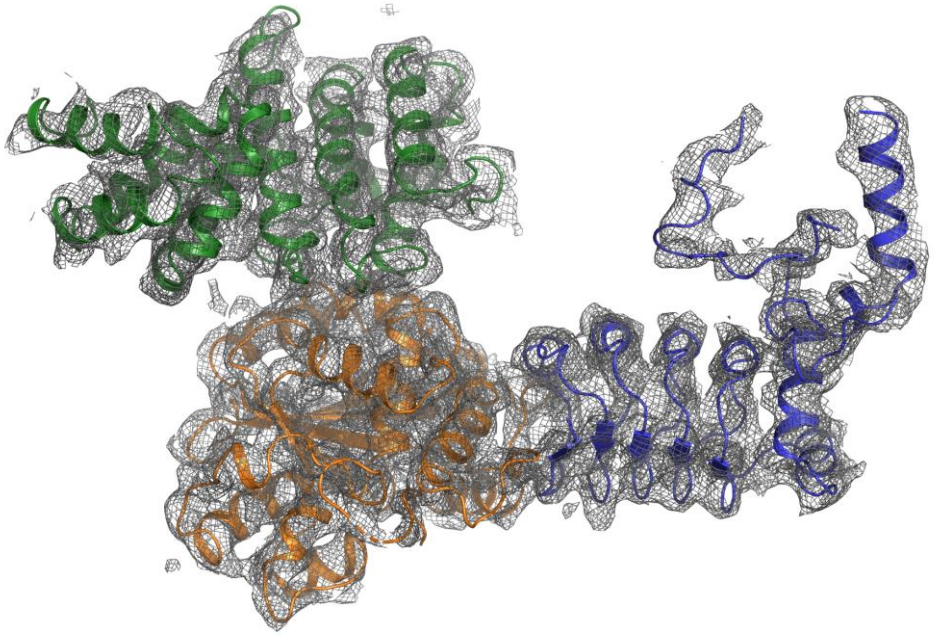

Figure S1. 2mFo-DFc difference electron density (contour: 1σ) covering the human CNOT1(MIF4G)-Caf1-Ccr4 structure. *Green*, CNOT1 (MIF4G) domain; *orange*, Caf1; *blue*, Ccr4/CNOT6L.

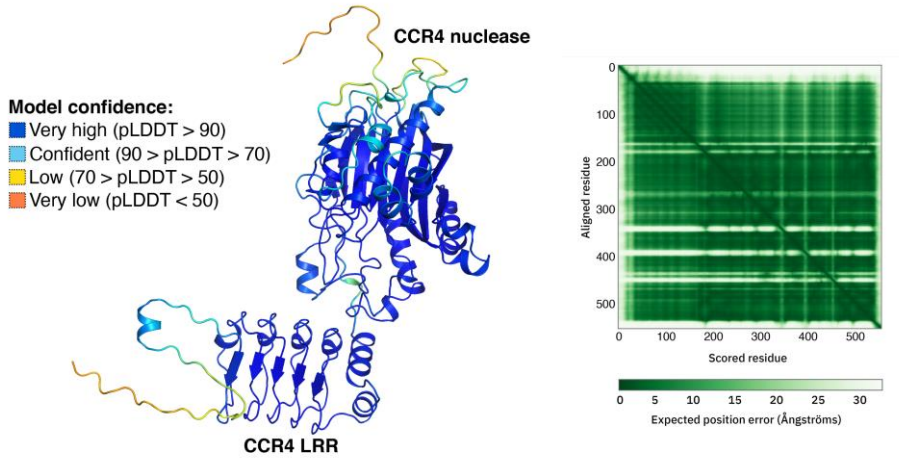

Figure S2. AlphaFold predicted structure of human Ccr4/CNOT6L. The structure figure was drawn using PyMOL and coloured according to confidence level (7). The right-hand panel was obtained via the AlphaFold server (8) at EMBL-EBI (9), which is reproduced under the CC-BY-4.0 licence.

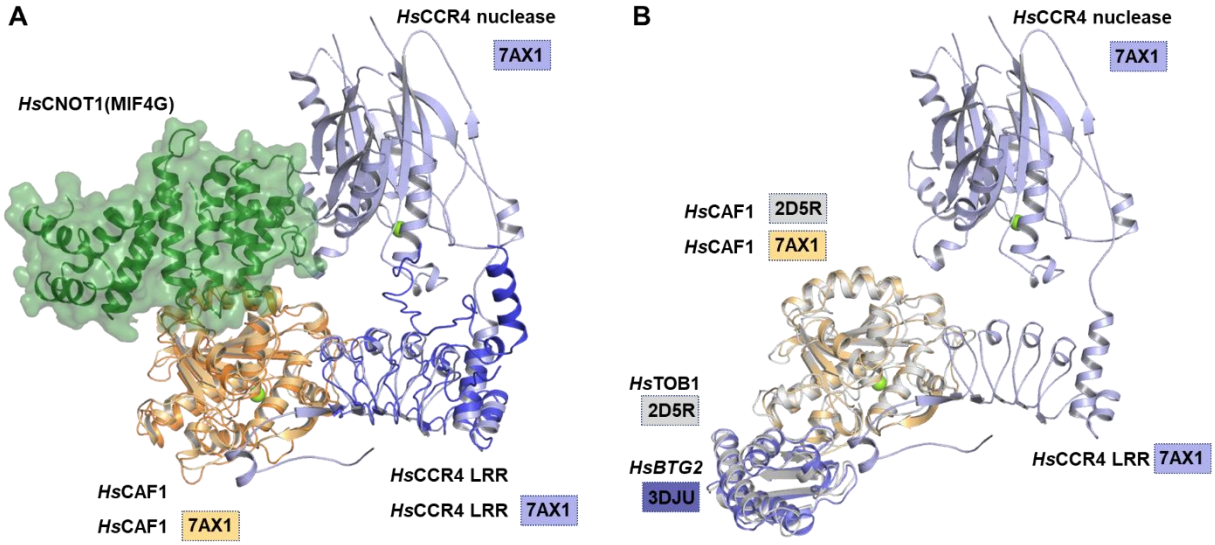

Figure S3. Superimposition of the human (*Hs*) Caf1-Ccr4 structure with human CNOT1-Caf1-Ccr4 and Caf1-Tob1 structures. **(A)** Superimposition of the human (*Hs*) Caf1-Ccr4 structure (PDB ID: 7AX1) (10) onto the human CNOT1-Ccr4-Caf1 structure. **(B)** Superimposition of the human (*Hs*) Caf1-Ccr4 structure (PDB ID: 7AX1) (10) onto the human Caf1-Tob1 structure (PDB ID: 2D5R) (11). The superimposed structure of the BTG2 protein (PDB ID: 3DJU) is also shown.

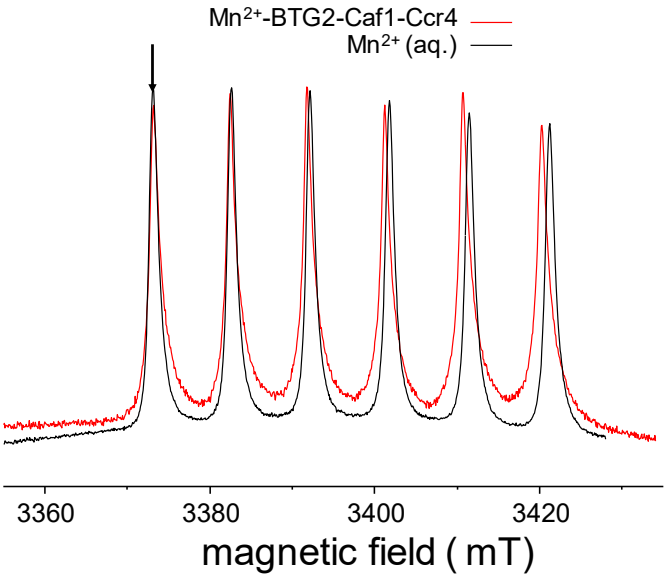

Figure S4. Field-sweep pulse EPR spectra of Mn^{2+} ions. The spectra in an aqueous solution of $MnCl_2$ (*black*) and Mn^{2+} bound to BTG2-Caf1-Ccr4 (*red*) are shown. Indicated is the position of magnetic field for RIDME measurements shown in Fig. 1E of the main text (*black arrow*).

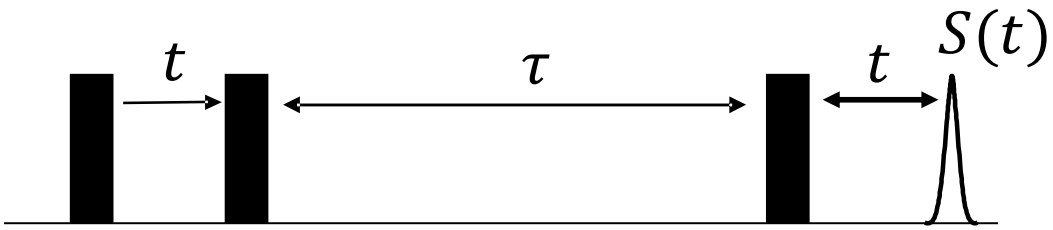

Figure S5. Three pulse version of relaxation induced dipolar modulation experiment (RIDME). The echo intensity $S(t)$ is recorded as a function of evolution time t. Due to electron spin relaxation taking place during the long mixing interval τ, the $S(t)$ undergoes dephasing due to flips of the neighbouring dipolar coupled electron spins.

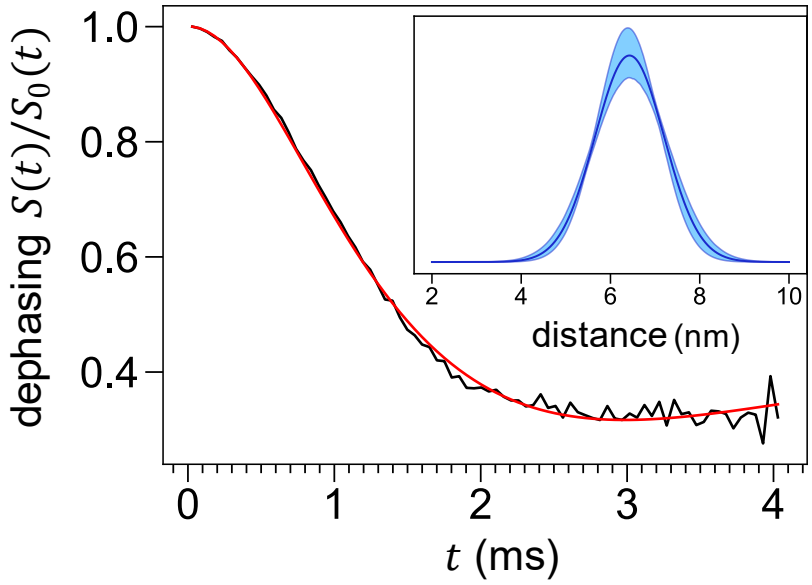

Figure S6. Normalized and background corrected RIDME trace for Mn^{2+} bound to BTG2-Caf1-Ccr4 complex, mixing time $\tau = 50$ µs. (Black line). The best fit result obtained using the distance distribution shown in the inset (red line). *Inset*: The distance distribution (*solid blue*) and the confidence interval corresponding to 95% (*light blue shade*).

Supplementary references

1. Abragam A, Bleaney B. 1970. Electron paramagnetic resonance of transition ions. The International Series of Monograms on Physics.
2. Epel B, Schafer KO, Quentmeier A, Friedrich C, Lubitz W (2005) Multifrequency EPR analysis of the dimanganese cluster of the putative sulfate thiohydrolase SoxB of Paracoccus pantotrophus. J Biol Inorg Chem 10:636-642. PMID: 16133204
3. Andersen KR, Jonstrup AT, Van LB, Brodersen DE (2009) The activity and selectivity of fission yeast Pop2p are affected by a high affinity for Zn^{2+} and Mn^{2+} in the active site. RNA 15:850-861.
4. Wang H, Morita M, Yang X, Suzuki T, Yang W, Wang J, Ito K, Wang Q, Zhao C, Bartlam M, Yamamoto T, Rao Z (2010) Crystal structure of the human CNOT6L nuclease domain reveals strict poly(A) substrate specificity. EMBO J 29:2566-2576.
5. Mullen GP, Serpersu EH, Ferrin LJ, Loeb LA, Mildvan AS (1990) Metal binding to DNA polymerase I, its large fragment, and two 3',5'-exonuclease mutants of the large fragment. J Biol Chem 265:14327-14334. PMID: 2201684
6. Pavanello L, Hall B, Airhihen B, Winkler GS (2018) The central region of CNOT1 and CNOT9 stimulate deadenylation by the Ccr4-Not nuclease module. Biochem J 475:3437-3450.
7. Schrödinger LLC The PyMOL Molecular Graphics System, Version 2.4.2.
8. Jumper J, Evans R, Pritzel A, Green T, Figurnov M, Ronneberger O, Tunyasuvunakool K, Bates R, Žídek A, Potapenko A, Bridgland A, Meyer C, Kohl SAA, Ballard AJ, Cowie A, Romera-Paredes B, Nikolov S, Jain R, Adler J, Back T, Petersen S, Reiman D, Clancy E, Zielinski M, Steinegger M, Pacholska M, Berghammer T, Bodenstein S, Silver D, Vinyals O, Senior AW, Kavukcuoglu K, Kohli P, Hassabis D (2021) Highly accurate protein structure prediction with AlphaFold. Nature 596:583-589.
9. Deepmind Technologies Limited. CCR4-NOT transcription complex subunit 6-like AlphaFold structure prediction. https://www.alphafold.ebi.ac.uk/entry/Q96LI5
10. Chen Y, Khazina E, Izaurralde E, Weichenrieder O (2021) Crystal structure and functional properties of the human CCR4-CAF1 deadenylase complex. Nucleic Acids Res 49:6489-6510. PMID: 34038562
11. Horiuchi M, Takeuchi K, Noda N, Muroya N, Suzuki T, Nakamura T, Kawamura-Tsuzuku J, Takahasi K, Yamamoto T, Inagaki F (2009) Structural basis for the antiproliferative activity of the Tob-hCaf1 complex. J Biol Chem 284:13244-13255. PMID: 19276069